JOURNAL OF GUIDANCE, CONTROL, AND DYNAMICS
Vol. 32, No. 6, November–December 2009

Role of Invariant Manifolds in Low-Thrust Trajectory Design

Rodney L. Anderson*
University of Colorado at Boulder, Boulder, Colorado 80309-0431
and
Martin W. Lo†
Jet Propulsion Laboratory, California Institute of Technology, Pasadena, California 91109

DOI: 10.2514/1.37516

This paper demonstrates the significant role that invariant manifolds play in the dynamics of low-thrust trajectories moving through unstable regions in the three-body problem. It shows that an optimization algorithm incorporating no knowledge of invariant manifolds converges on low-thrust trajectories that use the invariant manifolds of unstable resonant orbits to traverse resonances. It is determined that the algorithm could both change the energy through thrusting to a level where the invariant manifolds could more easily be used, as well as use thrusting to move the trajectory along the invariant manifolds. Knowledge of this relationship has the potential to be very useful in developing initial guesses and new control laws for these optimization algorithms. In particular, this approach can speed up the convergence of the optimization process, retain the essential geometric and topological characteristics of the initial design, and provide a more accurate estimate of the ΔV and fuel usage based on the initial trajectory.

Introduction

THE use of low thrust in trajectory design can significantly increase the complexity of the design process, because many of the standard astrodynamics tools are no longer applicable without what are sometimes significant modifications. For modeling performed in the two-body problem, the use of low thrust increases the difficulty of design in that the resulting trajectory no longer follows conic sections. In the three-body problem, the energy, or the Jacobi constant, changes because of the continuous thrust. As a result of these difficulties, much of the design work for low-thrust missions is performed using optimization tools which do not necessarily incorporate a full knowledge of the dynamics of the problem in the search for a desired trajectory. It has been observed, however, that the solutions developed using the Mystic optimization software [1–3] appear to generally follow the same types of paths as the invariant manifolds of unstable periodic orbits in the three-body problem [4]. This suggests that a knowledge of the relationship of these optimized trajectories to the invariant manifolds of unstable orbits could prove to be useful in the design of low-thrust trajectories. The long periods of time often required to run the optimization software could be significantly reduced if a good initial guess could be developed using the dynamics of the problem based on the invariant manifolds of the relevant unstable orbits. In this paper, we demonstrate how invariant manifolds play a central role in optimized low-thrust trajectories.

This paper arose from a study to understand optimized low-thrust trajectories for multimoon tours from a dynamical systems perspective. It specifically concentrates on the relationship of optimized low-thrust trajectories to the invariant manifolds of resonant orbits. The results given in this paper summarize the low-thrust results originally presented in a series of papers from 2004 to 2006 [5–7]. A more detailed version of these results may be found in Anderson's dissertation (2005) [8]. Our stated goals in this work have been to demonstrate that invariant manifolds do indeed play a role in low-thrust trajectories and to explain how the dynamics of low-thrust interplanetary trajectories interact with invariant manifolds. Lo et al. [5] compared low-thrust trajectories to the invariant manifolds of nearby unstable orbits at a single energy level. The outcome of this work suggests heuristically that we are on the right track, but, because low-thrust trajectories are constantly changing their Jacobi energy while thrusting, one must study a continuum of invariant manifolds in the energy range of the low-thrust trajectory. To do this, we must first understand the role of resonant orbits in planetary flybys and whether invariant manifolds play a role or not. For these reasons, in Anderson and Lo [6], we analyzed the planar Europa Orbiter (PEO) trajectory and found that it indeed follows the stable and unstable manifolds of the resonant orbits between impulsive maneuvers. In particular, it was found that the locations where the manifolds intersect in configuration space but not in phase space are the locations where a maneuver is required for moving from one manifold to another. This result suggests that a deeper understanding of the geometry of the invariant manifolds of resonant orbits is critical to understanding planetary flybys, and we anticipate this to also be true for low-thrust trajectories when they are moving through resonant orbit regions. These conjectures were found to be true, and the close relationship between low-thrust trajectories and the invariant manifolds of unstable resonant orbits was shown in Lo et al. [7]. Since that time, subsequent research has been performed by several groups building on the optimization techniques developed by Lawden [9], Betts and Erb [10], and Betts [11]. In addition to this work, several of these researchers have begun to focus on optimization within a multibody environment, particularly with regard to using libration point orbits. Whiffen and Lam have continued to develop and apply the Mystic software to missions such as the Jupiter Icy Moons Orbiter [12] and the Dawn mission. Howell's group has applied optimization techniques to trajectories with gravity flybys and looked at low-thrust trajectories transferring to libration point orbits in the Earth–moon system [13,14]. Dellnitz et al. used the concept of reachable sets in combination with the invariant manifolds of libration orbits to look at a low-thrust transfer from Earth to Venus [15].

Studying low-thrust trajectories in this type of environment continues to be a vibrant area of research, and this fact emphasizes the importance of continuing to explore these trajectories in a three-body environment. The role of resonance transition that our papers have focused on continues to be important for understanding trajectories within the context of this problem. In this paper, we examine and summarize the relationship between a low-thrust trajectory and the invariant manifolds of several families of resonant orbits through the energy levels traversed by the low-thrust trajectory.

Received 13 March 2008; accepted for publication 10 February 2009.

*Research Associate, Colorado Center for Astrodynamics Research, Aerospace Engineering Sciences, Campus Box 431. Member AIAA.
†Senior Engineer, 4800 Oak Grove Drive. Member AIAA.

Models and Tools

Circular Restricted Three-Body Problem

The circular restricted three-body problem (CRTBP) was the primary model used in this study. In this model, two bodies, typically referred to collectively as the primaries, are assumed to rotate about their center of mass in circular orbits, and the objective is to describe the motion of a third infinitesimal mass placed in this system. This infinitesimal mass could represent a spacecraft, asteroid, comet, or dust particle. If the infinitesimal mass is restricted to the plane of motion of the two primaries, the problem is called the planar CRTBP. In formulating the equations of motion for the infinitesimal mass, the required quantities are usually normalized and nondimensionalized so that the mass of the smaller body (the primary) is μ, and the larger body (the secondary) has mass $1-\mu$. The distance between the two bodies becomes one with the primary located on a rotating x axis at $x_1 = -\mu$ and the secondary at $x_2 = 1-\mu$. The dimensionless time corresponds to the angle between the x axis of the rotating frame (defined so that the x axis always passes through the two bodies) and the x axis of the inertial frame. The period of the rotating system becomes 2π. Both the mean motion and the gravitational constant are one. Using this notation, the equations of motion for the infinitesimal mass in the rotating system may be written as

$$\ddot{x} - 2\dot{y} = x - (1-\mu)\frac{x-x_1}{r_1^3} - \mu\frac{x-x_2}{r_2^3}$$

$$\ddot{y} + 2\dot{x} = \left(1 - \frac{(1-\mu)}{r_1^3} - \frac{\mu}{r_2^3}\right)y \qquad \ddot{z} = -\left(\frac{(1-\mu)}{r_1^3} - \frac{\mu}{r_2^3}\right)z \quad (1)$$

Here, the distances from the infinitesimal mass to the primary and secondary are r_1 and r_2, respectively. The x axis location of the primary is x_1 and that of the secondary is x_2. An energylike integral of motion called the Jacobi constant exists in this model, which varies when maneuvers are performed. It may be computed as

$$C = x^2 + y^2 + \frac{2(1-\mu)}{r_1} + \frac{2\mu}{r_2} - \dot{x}^2 - \dot{y}^2 \quad (2)$$

Finally, there are five equilibrium points in the problem (the Lagrange points) about which periodic orbits exist. See Szebehely [16] or Roy [17] for detailed descriptions of the CRTBP.

Poincaré Maps

Poincaré maps are useful for studying complicated systems because they bring out information that would otherwise be obscured. To compute a Poincaré map for a system in $\mathbb{R}^n$, a "hypersurface" Σ, or surface of section in $\mathbb{R}^{n-1}$ is placed transverse to the flow, as shown in Fig. 1. A trajectory intersecting the surface of section is integrated until it intersects the surface of section once again. The mapping is from the first intersection to the next intersection and so on. The points of the mapping may then be plotted using a number of different coordinates, although only some coordinates will result in visible structure. Given the planar CRTBP in $\mathbb{R}^4$, the surface of section is specified by fixing one of the coordinates to produce a surface in $\mathbb{R}^3$. For example, given a particular case where the surface of section is defined so that y is always zero, the coordinates x and $\dot{x}$ are quite commonly used. These Poincaré surface of sections or Poincaré sections bring out a surprising amount of detail, which allows the location of stable periodic and quasi-periodic orbits to be computed.

In this analysis, the surface of section is specified by $y = 0$ along the x axis opposite Europa (as shown later). The Jacobi constant is fixed for all the points in the Poincaré section, which means that the resulting surface of section is two-dimensional. So, with x defined, $\dot{x} = 0$ and $y = 0$. The magnitude of $\dot{y}$ can then be calculated in the planar problem from the Jacobi constant as

$$\dot{y} = \pm\sqrt{x^2 + y^2 + \frac{2(1-\mu)}{r_1} + \frac{2\mu}{r_2} - \dot{x}^2 - C} \quad (3)$$

As mentioned previously, resonant orbits and their invariant manifolds are of particular importance to this analysis, and their intersections with the surface of section are computed throughout this paper. It is also useful to compare these resonant orbits and invariant manifolds with the typical Poincaré section showing the stable quasi-periodic orbits and other structures at different resonances. These background points showing the quasi-periodic orbits and other structures were computed by starting with a set of initial conditions in an equally spaced grid on the x axis and integrating them forward in time. The first two intersections of each trajectory with the x axis were discarded to allow the dynamics to remove the effect of the grid, but the remaining intersections were used in the Poincaré section. For this analysis, only those points crossing the surface of section with a positive $\dot{y}$ were plotted because only the resonant orbits crossing the $y = 0$ line with $-x$ values were of interest. Generally, the initial set of points were selected based on approximations from the two-body equations and the desired surface of section. Usually the initial $\dot{x}$ was set equal to zero, but $\dot{x}$ was given a value of 0.05 when the main resonances of even order were of interest. See Murray and Dermott for the rationale behind this technique [18]. A Runge–Kutta Fehlberg seventh-order integrator with stepsize control was used to generate the Poincaré sections. If the Jacobi constant was found to vary more than approximately 10^{-3}, it generally indicated a close approach to one of the singularities. The integration was stopped, and the integrator proceeded on to the next point in the grid. This approach was favored over using regularization to save time, and it had no negative consequences, as it was only used to generate the background points in the Poincaré surface of sections.

Invariant Manifolds

A manifold may be most simply defined as an m-dimensional surface embedded in $\mathbb{R}^n$ which locally possesses the structure of $\mathbb{R}^m$ [19]. The term "invariant" indicates that a trajectory of a point on the manifold will remain on the manifold as time evolves. Invariant manifolds may be subdivided into stable and unstable manifolds. Simply speaking, a stable manifold for a flow consists of those points that approach a limit set L as time moves forward toward infinity, whereas an unstable manifold consists of the points that approach the limit set as time moves backward. A limit set for these purposes is a periodic orbit or an equilibrium point. More formally, the stable and unstable manifolds for a flow ϕ_t are as follows:

The stable manifold $W^s(L)$ is the set of points x such that $\phi_t(x)$ approaches L as $t \to \infty$.

The unstable manifold $W^u(L)$ is the set of points x such that $\phi_t(x)$ approaches L as $t \to -\infty$.

See Parker and Chua [20] for more details.

In calculating the stable and unstable manifolds of a libration or resonant orbit, the fact that these orbits are periodic is used to discretize the continuous time system and form a map. The Poincaré maps discussed earlier, where a surface Σ is constructed transverse to the flow at a particular point, are often used for this purpose. Refer back to Fig. 1 for an example of the three-dimensional case. Using this method, a trajectory intersects the surface at intervals of time corresponding to approximately one period. This process reduces the problem to a lower-dimensional problem and aids in the study of the dynamics of the orbit. A truly periodic orbit would return to the same point on the Poincaré map each time it intersected the surface. Such a point is referred to as a fixed point, and its map can be examined to understand stability. A similar concept is that of a stroboscopic map where the flow is observed at intervals equal to the period of the orbit [20]. In this case, the state transition matrix from the initial time t_o to

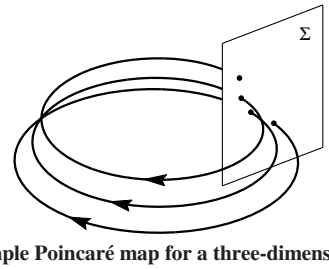

Fig. 1 Sample Poincaré map for a three-dimensional system.

the time after one period ($t_o + T$) is referred to as the monodromy matrix and is designated by $\Phi(t_o + T, t_o)$. The stability characteristics of this point on the libration trajectory may be evaluated by examining the eigenvalues and eigenvectors of this matrix. The algorithm for computing manifolds uses the fact that the eigenvector corresponding to an eigenvalue greater (less) than one is in the direction of the local unstable (stable) manifold. To compute the manifold, an initial point corresponding to an offset of approximately 1.0×10^{-6} dimensionless units in the direction of the desired eigenvector is calculated [21]. This offset may be taken either in the direction of the calculated eigenvector or in the opposite direction. One direction typically takes the trajectories toward the secondary and one will usually cause them to travel in the opposite direction. For calculation of the unstable manifold, the trajectory is then integrated forward in time from the given point, and for the stable manifold, the trajectory is integrated backward in time.

Visualization of the Low-Thrust Trajectory Relative to the Invariant Manifolds

The inclusion of low thrust and the corresponding variations in energy into the analysis introduces a number of significant challenges in terms of visualizing the trajectory and its relationship to the relevant dynamical structures. Ideally, a complete examination could be achieved by comparing the trajectories to the invariant manifolds at each energy level in phase space, but this turns out to be a rather difficult proposition for higher-dimensional systems such as the CRTBP.

Even in previous work where a trajectory at only one or very few energy levels was examined, this sort of comparison was found to be difficult to visualize [6]. In these cases, the resonant orbits and their invariant manifolds were computed at the same Jacobi constant as the trajectory. Then the dimension of the problem was reduced through the use of a Poincaré section (see the Poincaré map section). The intersections of the invariant manifolds with the Poincaré section was computed, and the intersection of the trajectory was plotted for visual comparison. It is worth reiterating that this method allows for a complete comparison of the trajectory and the invariant manifolds in the planar CRTBP, because fixing the Jacobi constant of all points in the Poincaré section means that points at the same location in the Poincaré section have the same state.

One option with the addition of low thrust would be to use the same procedure as for impulsive trajectories where the intersection of the trajectory with the surface of section is compared to the invariant manifolds at that energy. However, this option would ignore the other points on the trajectory which possess different energies. One possible way to perform the comparison, illustrated in Fig. 2, would be to compute new Poincaré sections that intersect each individual point on the trajectory. For each of these Poincaré sections, the intersections of the resonant orbits and their invariant manifolds would be recomputed at the instantaneous energy of the selected point on the trajectory. This method, however, becomes awkward when a comparison of the Poincaré sections is desired because the invariant manifolds evolve in space. So the comparison is difficult because the invariant manifolds are being compared at different locations and at different energies.

One solution to this problem, illustrated in Fig. 3, is to use only one Poincaré section fixed in space and map the instantaneous state of the spacecraft back to the surface of section for each point along the trajectory. The invariant manifolds of the resonant orbits would be recomputed for each energy level, but, in this case, the dynamical structures in each Poincaré section could be directly compared, with the only difference being the energy. Note that the mapping is achieved using integration without the inclusion of the thrusting force. If the thrust was included in the mapping, then every point on the trajectory would simply map back to the same single point. The comparison of this point with the invariant manifolds computed at the energy of the instantaneous point along the trajectory would be invalid because the energies would be different. Also worth mentioning is the fact that the mapping is shown in only one direction

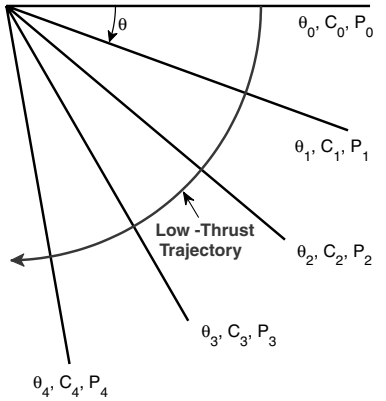

Fig. 2 Illustration of multiple Poincaré sections P_i, computed at different energies, intersecting the trajectory. Each Poincaré section is computed at the instantaneous energy of the trajectory. Multiple Poincaré sections at different locations are required.

in Fig. 3. It is possible to either map the instantaneous state on the trajectory back in time to the surface of section, or it could also be mapped forward in time until it intersected the surface of section once again. The intersections would typically not be the same unless the instantaneous point lies on a periodic orbit. The change in the intersections in this case represents the natural evolution of a ballistic trajectory under the dynamics of the system from one intersection to the next. Both intersections contain potentially useful information, and the use of both will be explored here.

This second method was chosen for this study because it eliminates the spatial variations in the invariant manifolds and allows a comparison of the changes in the dynamical structures as a function of energy alone. It must be remembered that the points in this method still cannot be compared directly. They must be compared relative to the changing invariant manifolds at each energy level. These techniques will be further developed and applied to an optimized low-thrust trajectory in the Jovian system next.

Planar Ganymede to Europa Trajectory

This analysis focuses on a nearly planar low-thrust trajectory (developed by Lam [22] using Mystic) which travels from near Ganymede to Europa in the Jupiter–Europa CRTBP. This trajectory was optimized primarily with the goal of minimizing the expended propellant, but the initial reference trajectory that the initial conditions were taken from also incorporated a number of mission design constraints. For more details on the initial reference trajectory see Whiffen and Lam [12]. Although the trajectory was developed within the Jupiter–Europa system, it is expected that the results

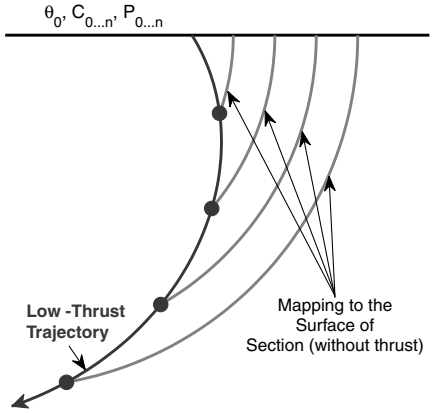

Fig. 3 Illustration of Poincaré sections computed at the same location for different energies. Each instantaneous point on the trajectory is mapped to the surface of section. The intersections are not at the same point as the low-thrust trajectory because the mapping is achieved via integration where the thrust is not included.

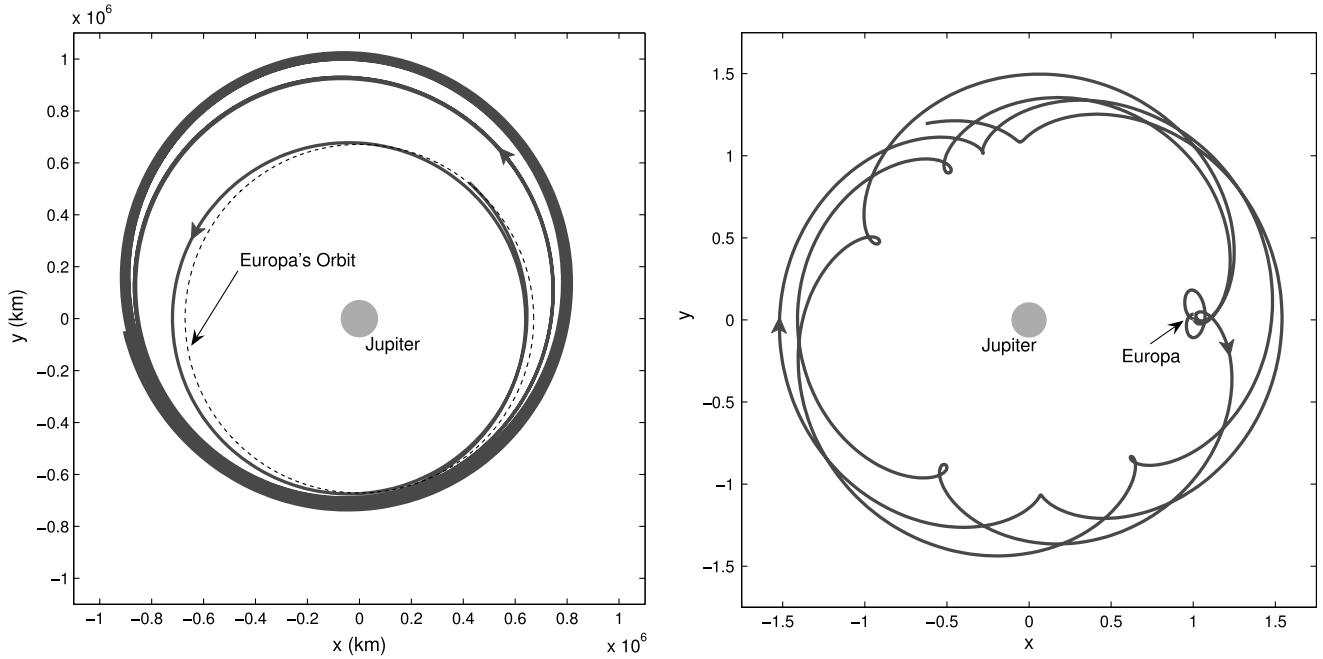

a) Inertial frame **b) Jupiter-Europa rotating frame**

Fig. 4 Planar low-thrust trajectory traveling from near Ganymede to Europa.

presented in this study will be generally applicable to missions designed within the context of other systems in the three-body problem. The Mystic software itself implemented the static/dynamic optimal control algorithm, which is a nonlinear optimal control method used to optimize static and dynamic variables at the same time. More information on both Mystic and the underlying algorithms may be found by referring to Whiffen [1,3]. The trajectory analyzed in this study is shown in both the inertial and rotating frames in Fig. 4. As mentioned previously, the convergence process in Mystic did not allow the trajectory to remain completely planar, but the maximum deviation from the plane was only 7.4 km or 1.1×10^{-5} dimensionless distance units. This was judged to be sufficiently planar so that the previously developed techniques based on using Poincaré sections in the planar CRTBP should still be adequate for this analysis [5–7]. Examining the trajectory in the inertial frame indicates the possible presence of three distinct periods or resonances. The variation in the number of loops on the trajectory in the rotating frame also confirms that the trajectory is traveling through at least two resonances. This observation is not as clear as in the case of the impulsive PEO trajectory analyzed previously [5,6], as the energy is changing continuously along multiple sections of the trajectory rather than just at two points. Finally, the trajectory as it approaches Europa appears to possess the characteristics of a distant retrograde orbit (DRO). See Lam and Whiffen [23] for a detailed study of DROs in the Jupiter–Europa system, but they may briefly be described as stable, periodic orbits traveling in a retrograde motion about Europa in the rotating frame.

The effect of low thrust on the characteristics of the trajectory may be quantified using both two-body and three-body parameters. The shaded regions in Fig. 5 indicate the times when multiple extended periods of thrusting occurred. During these times, the thrust was almost always at approximately 2500 mN. Even during the regions that appear to be gaps, thrusting on the order of 1.0 mN takes place. Examining the Jacobi constant in Fig. 5 confirms the expectation that the Jacobi constant undergoes its major changes during periods of higher thrusting. The slight changes observed in the other regions are due to the fact that some small thrust is still being applied. At first it seems curious that, unlike the PEO, this trajectory is traveling from a higher Jacobi constant to a lower Jacobi constant. However, it should be noted that the low-thrust trajectory is traveling from Ganymede which would generally have a high Jacobi constant of approximately 3.15 if it were computed in the Jupiter–Europa system. The PEO is attempting to approach Europa from a more energetic trajectory which would correspond to a lower Jacobi constant. The two-body period in Fig. 5 appears to undergo some changes as a result of the thrusting, but the variations elsewhere along the trajectory arise from the three-body perturbations. Note that the two-body period was computed with respect to the barycenter. These results are consistent with those of the PEO, which saw changes in the period between ΔVs as a result of flybys.

Trajectories that have been previously analyzed [8] demonstrated a relationship with the invariant manifolds of unstable periodic orbits, therefore, it is expected that the low-thrust trajectory may possess a similar connection. Determining whether such a relationship exists requires the computation of the invariant manifolds of the correct unstable periodic orbits at each energy level found on the low-thrust trajectory. The relevant unstable orbits may be unknown initially, but, at least for resonant orbits, a guess as to the appropriate resonance may be obtained by using the two-body periods calculated along the trajectory.

First, however, the visualization techniques discussed earlier were implemented along this trajectory. The first step in this method involves the computation of the intersections with the surface of section[‡] of the instantaneous state on the low-thrust trajectory mapped forward and backward in time. In this process, the state at each point on the low-thrust trajectory was first selected neglecting the z components, which were nearly zero. This state was then mapped backward in time without thrust until it intersected the surface of section, and this point was recorded. Next, the same state was mapped forward in time without thrust until it intersected the surface of section. This is illustrated for a single point on the low-thrust trajectory in Fig. 6. Each of these points were then saved for comparison with the invariant manifolds corresponding to the energy of each point.

Although it is not strictly a valid comparison, these intersections were initially plotted in Fig. 7 for comparison in a rough sense. Examining these intersections by themselves does reveal structures that heuristically appear to be similar to the invariant manifolds computed for the PEO trajectory. This indicates the existence of a possible relationship to the invariant manifolds in at least a rough sense. To say anything more definitive, a more thorough analysis including the various dynamical structures at each energy level must be performed.

[‡]Note that the surface of section used throughout this paper is at the same location as shown in Fig. 6.

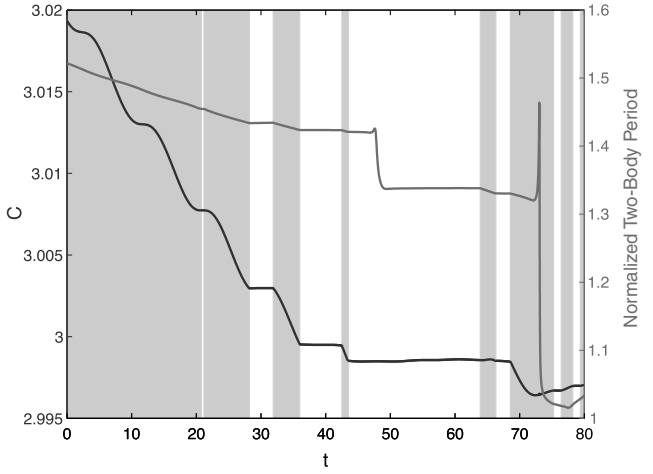

Fig. 5 Changes in three-body and two-body parameters compared to periods of thrusting. Gray shading indicates periods of significant thrust which, for this time period, were almost all at approximately 2500 mN. The dimensionless time is indicated by *t*.

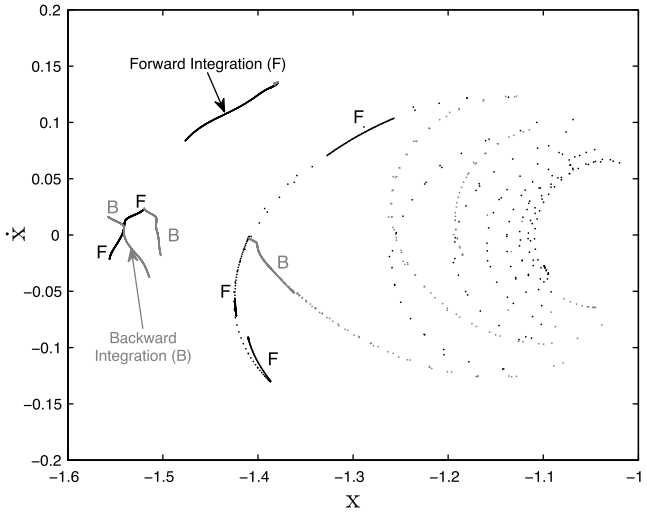

Fig. 7 Intersections with the surface of section of individual points on the low-thrust trajectory integrated forward and backward in time. The instantaneous state at each point on the trajectory was used in the integration, which did not include any thrust. It is important to note that the energy of each of these points is not the same, and this plot just provides a rough comparison. Each point is computed in the same manner as the points illustrated in Fig. 6.

Resonant Orbits

The primary dynamical structures of interest in this analysis are unstable resonant orbits and their invariant manifolds. In our case, the low-thrust trajectory appears to travel between different resonances, therefore, it is natural to expect the existence of a relationship between this trajectory and the three-body resonant orbits at these resonances. More specifically, the relationship to the resonant orbits possessing the same Jacobi constant is of interest. For Hamiltonian systems, resonant orbits do not appear in isolation but in continuous families. An initial guess for a resonant orbit at a desired resonance may be obtained using the integration of large numbers of orbits and Poincaré sections. Once this initial guess has been obtained, it may be converged to a truly symmetric periodic orbit about the x axis using standard single shooting techniques [24]. After the initial resonant orbit has been found, the problem is then to continue the orbit to obtain a resonant orbit at the desired energy. Although a wide variety of continuation techniques have been developed, a simple linear extrapolation of conditions along the x axis was found to be sufficient for this study of resonant orbits. Once a series of orbits across a range of Jacobi energies have been found, a simple secant method can be used to compute a resonant orbit at any desired energy value.

The continuation plots in Fig. 8 give a summary of the families of orbits found at the 3:4 and 5:6 resonances using the techniques just described. Each family is labeled first by the resonance. They are then labeled according to whether they pass through the inner (I) region between Jupiter and Europa or the outer (O) region. Finally, they are also labeled according to whether a loop exists on the line of syzygy (L) or not (N). Although not necessarily expected, it appears that several different types of unstable resonant orbits may exist at each resonance for a given energy level. In each case, the family was continued until the linear extrapolation method failed to converge on a trajectory in the same family. In these cases, the points on the continuation plot typically took an abrupt turn, as can be seen in Fig. 8b where the 5:6-NI family turns, and the family can no longer be continued using this method. This might be a sign of a bifurcation,

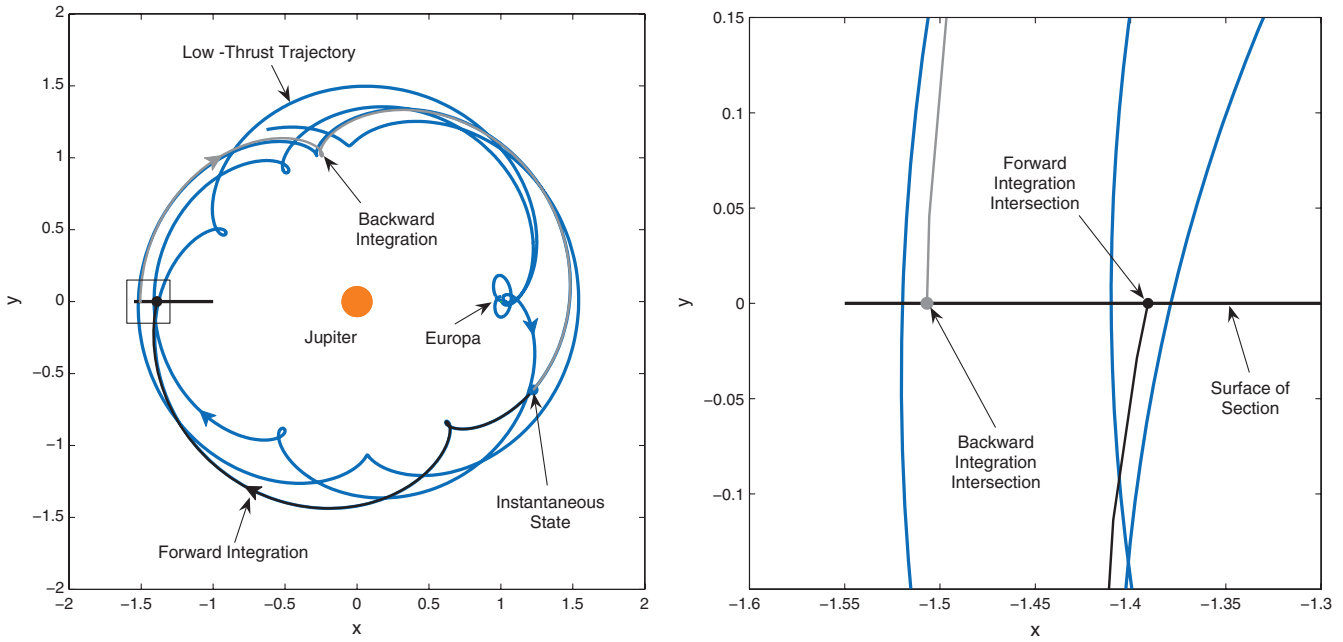

a) Trajectory overview **b) Boxed region**

Fig. 6 Illustration of the computation of the points in the Poincaré section for the low-thrust trajectory. The points integrated without thrust intersect the surface of section at different points from the low-thrust trajectory.

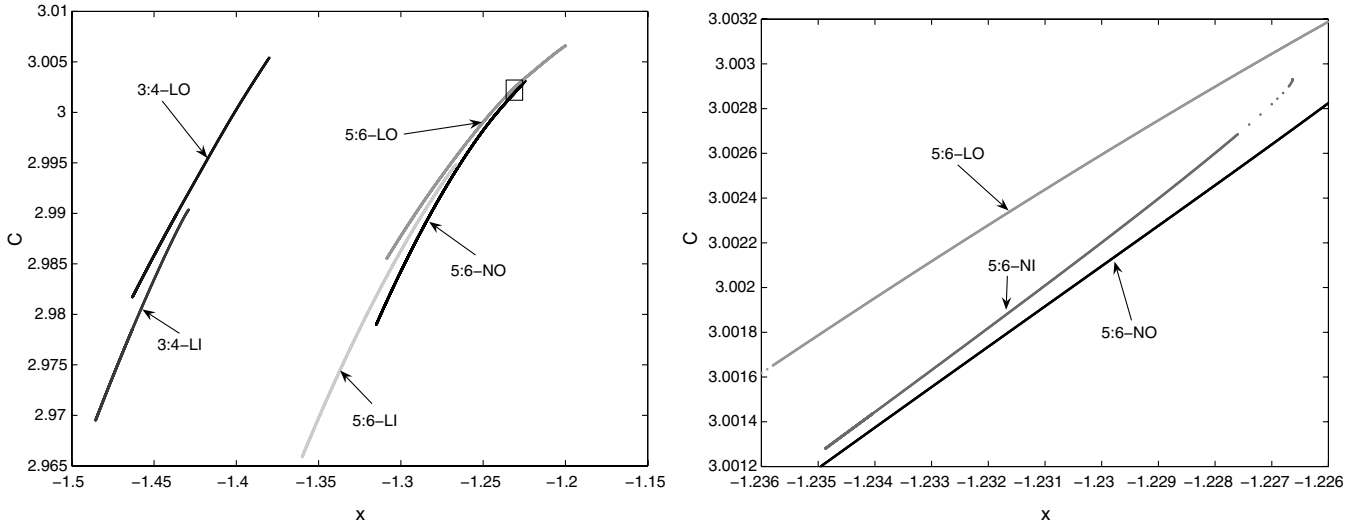

a) Continuation plot overview **b) Boxed region**

Fig. 8 Continuation plot for the 3:4 and 5:6 families of resonant orbits. The points represent the initial conditions on the *x* axis for each of the converged orbits.

but more sophisticated techniques would be required to analyze this phenomena which we ignore for the moment.

A selection of the converged orbits in the 3:4-LO and 5:6-LO families are shown in Figs. 9 and 10 at even intervals of energy. These families were found to be of the most interest for the given low-thrust trajectory. Note that limits in the continuation are often either the point where the family encounters Europa or where a change in the topology of the trajectory occurs. For a more detailed analysis of all of these families see Anderson [8].

Comparison with Invariant Manifolds

Ideally, a study of the relationship of the low-thrust trajectory to the invariant manifolds of unstable orbits would include a comparison in phase space of each instantaneous point on the trajectory with the invariant manifolds computed at the energy of that point. As mentioned previously, this approach quickly becomes cumbersome even in configuration space, making the use of Poincaré sections desirable. These Poincaré sections were computed for each of the desired points on the trajectory to understand how the low-thrust trajectory moved relative to the invariant manifolds as thrust was applied. The initial portion of the low-thrust trajectory contained points at Jacobi constants above the range computed for the unstable resonant orbit families. Therefore, this analysis starts approximately 14.3 days after the initial epoch on the low-thrust trajectory. The Poincaré sections computed for each point on the low-thrust trajectory were generally viewed as a movie, of which some of the frames are discussed shortly.

First though, it is worth examining a single frame of the movie, as shown in Fig. 11, to understand the relevant dynamical structures and how they relate to the low-thrust trajectory intersections. As explained previously, each frame corresponds to a specific Jacobi constant computed for a particular point on the low-thrust trajectory. This frame was computed for the point that was mapped to the

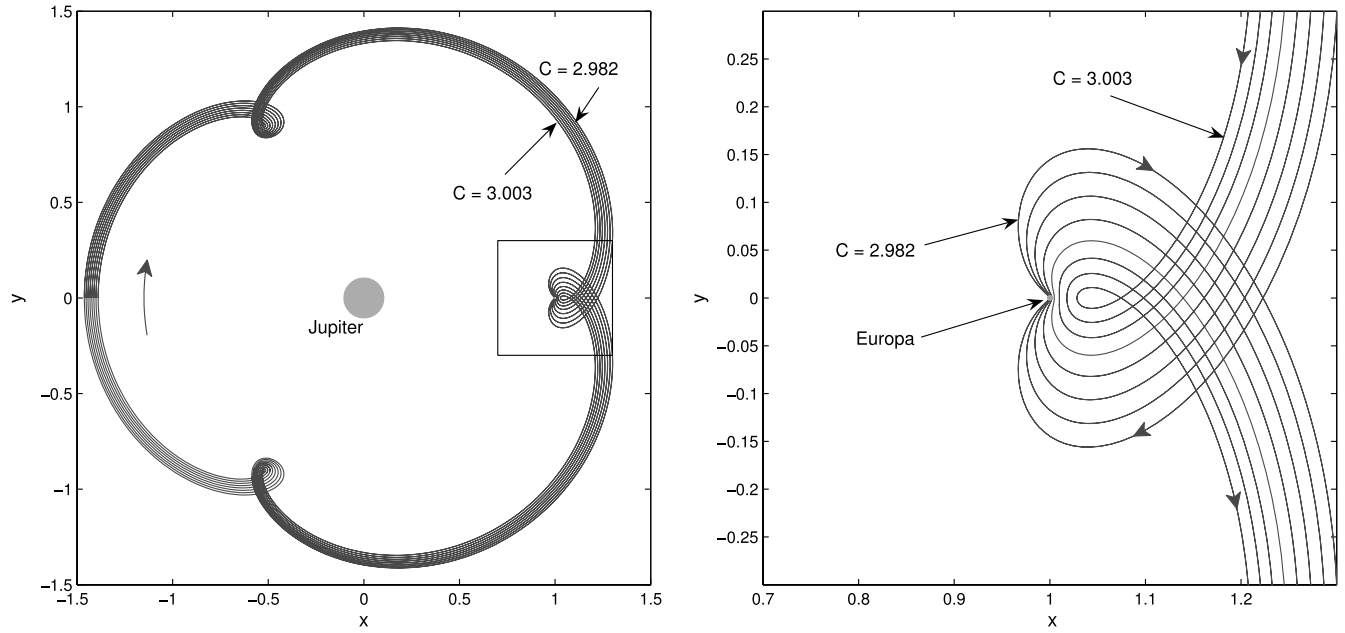

a) Resonant orbit family overview **b) Boxed region**

Fig. 9 Orbits in the 3:4-LO family. The Jacobi constant of the two bounding trajectories are labeled, and the intermediate trajectories vary linearly in their Jacobi constant in increments of 0.003.

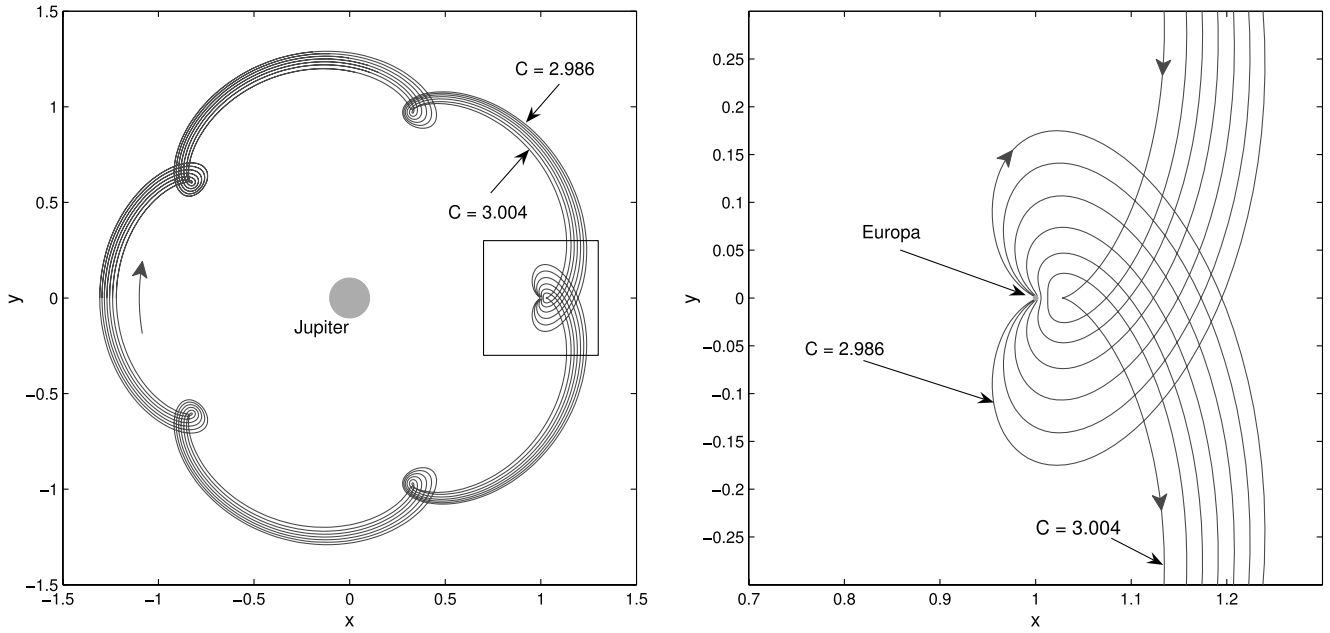

a) Resonant orbit family overview **b) Boxed region**

Fig. 10 Orbits in the 5:6-LO family. The Jacobi constant of the two bounding trajectories are labeled, and the intermediate trajectories vary linearly in their Jacobi constant in increments of 0.003.

surface of section and labeled as the starting point in the figure. The resonant orbits' intersections at the 3:4 and 5:6 resonances are plotted as labeled for the given Jacobi constant along with the intersections of each resonant orbit's stable ($W^s_{3:4}$, $W^s_{5:6}$) and unstable ($W^u_{3:4}$, $W^u_{5:6}$) manifolds. It is worth noting that this typical frame contains nearly 25,000 background points and approximately 35,000 points in the manifolds. Depending on the frame, the integration time can range from several minutes to a quarter hour. Generating a whole series of frames can take several hours, but once the frames are computed for a range of energies in a particular system there is no need to regenerate them. For the planar problem, the complete information for each trajectory is stored in the Poincaré section, and the data are easily stored for analysis.

One area of interest is how these structures vary as the trajectory and the Jacobi constant changes. Another is whether the trajectory will in any way follow the invariant manifolds for the appropriate energy level. To provide an initial answer to this first question, a series of intersections was chosen and plotted in Fig. 11 where some thrusting occurred but where the Jacobi constant was not changing dramatically. Over this period, the background points and intersections of the

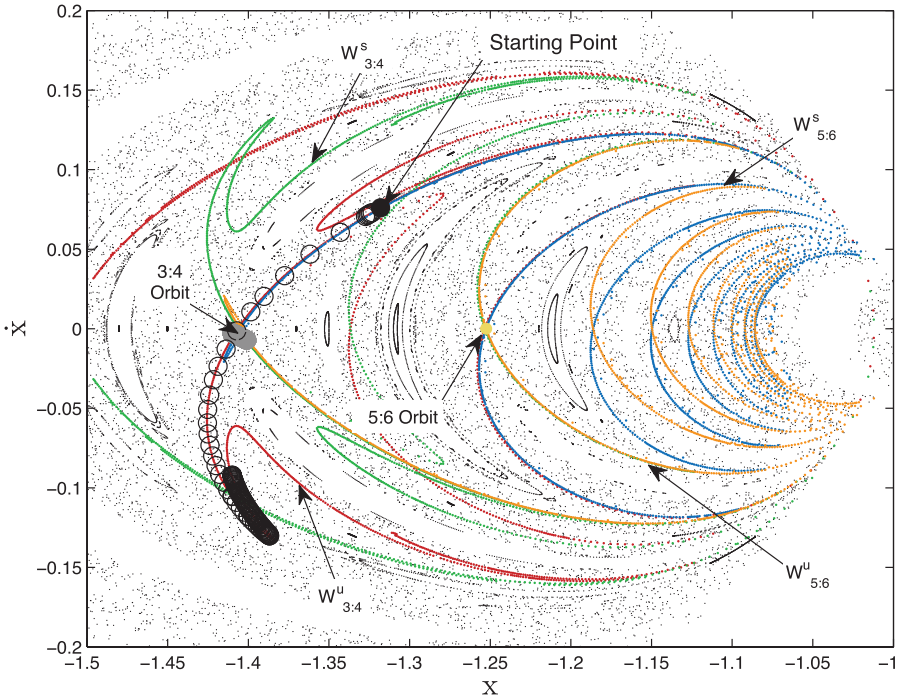

Fig. 11 Summary plot showing the resonant orbits and invariant manifold intersections computed at the Jacobi constant of the starting point. The black circles indicate the intersections of the forward integrated points, and the gray circles represent the backward integrated points. All of the black and gray points are at similar but slightly different Jacobi constants. Only the outline of the black and gray points are shown here so as not to obscure the invariant manifolds. The areas where the points appear solid have many adjacent points.

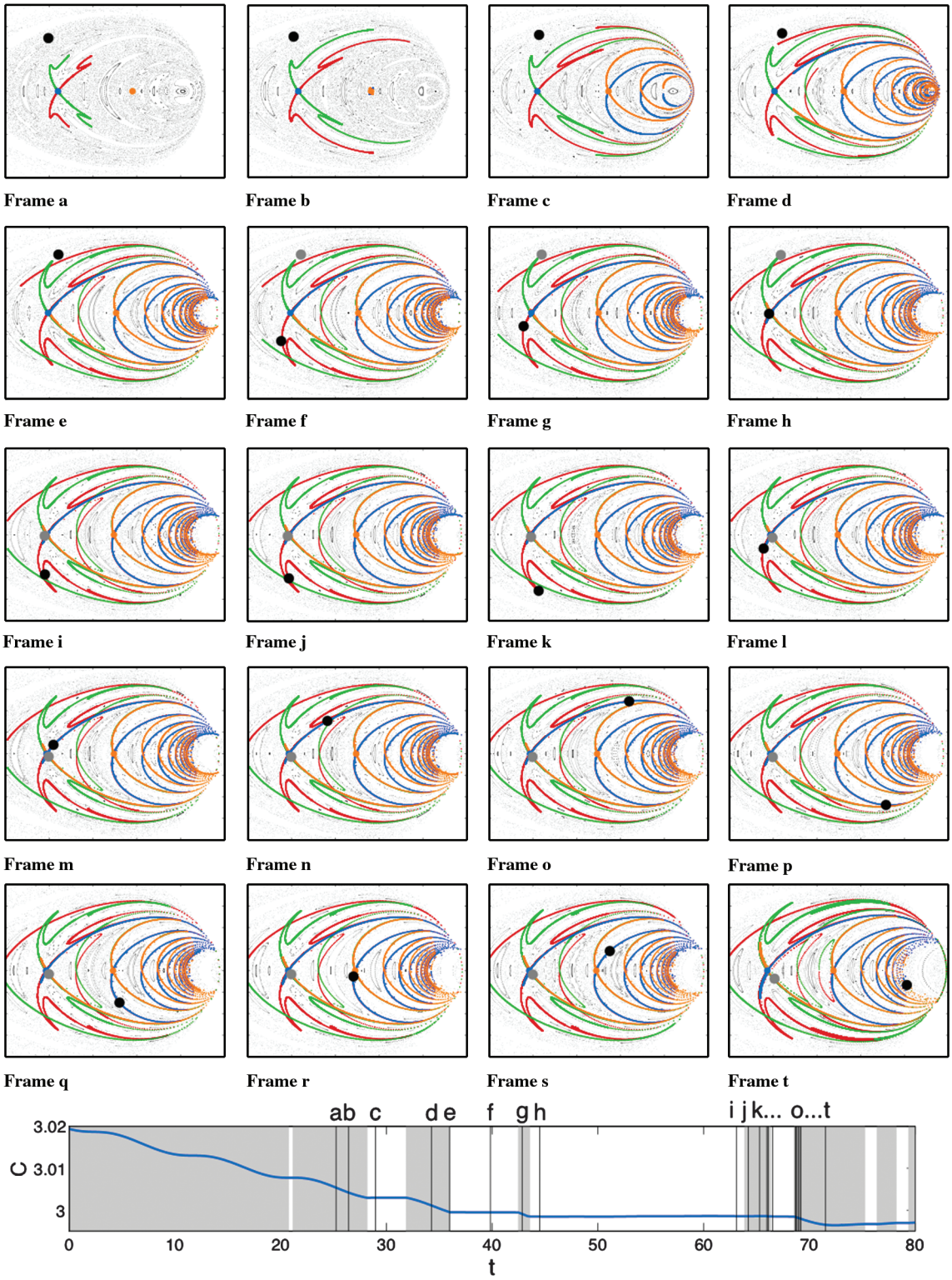

Fig. 12 Poincaré sections (*a*–*t*) for various points on the low-thrust trajectory. Once again, the black and gray points are the forward and backward integrated points, respectively. The labels on the axes are removed for easier visualization, but they have the same limits as used in Fig. 11. The same colors are also used for the resonant orbits and their invariant manifolds. The vertical lines on the Jacobi constant plot (bottom) indicate the times corresponding to each Poincaré section which are plotted sequentially. So the frames vary in both time and Jacobi constant, and the intersection of the vertical lines with the Jacobi constant curve gives the instantaneous Jacobi constant for each frame. A standard time interval was used to compute the invariant manifolds in each frame, and the invariant manifolds in frames *a* and *b* do not extend as far as the other frames because of the energy level. A longer time interval would be required to extend the invariant manifolds further at these energy levels.

dynamical structures changed only incrementally, therefore, a comparison of the points over this time with the background points at the energy level of one of the points is judged to be valid. The result when the points mapped forward (black) and backward (gray) are plotted relative to the invariant manifolds is striking. During this time period, all of the forward intersections lie very near the unstable manifold of the 3:4 orbit. In other words, the optimizer has chosen to thrust in such a way that its solution follows the invariant manifold of the 3:4 resonant orbit. The fact that the trajectory follows the exact shape of the invariant manifold out of all potential paths indicates a clear relationship between the optimized low-thrust trajectory and the invariant manifolds.

Altering the Invariant Manifold Structure by Changing *C*

The first frame shown in Fig. 12 starts off at the highest Jacobi constant in this analysis.[§] The same convention introduced earlier holds here where a black point represents a state on the low-thrust trajectory integrated forward, while a gray point represents a backward integration. Now, however, only the two points corresponding to the energy level of the specified Poincaré section are plotted for each frame.

In the first frame, the point obtained from the backward integration is not visible as it is to the left of the plot, but the forward integration gives a point somewhat distant from the invariant manifolds. It is suspected that it might lie close to the invariant manifold of another unstable resonant orbit that was simply not computed for this study. As time progresses though, the stable invariant manifold of the 3:4 resonant orbit appears to approach the forward integration intersection as it also moves slightly. In frame *g*, as the point integrated backward comes closer to the stable manifold of the 3:4 resonant orbit, the forward integrated point is found to lie nearer the 3:4 resonant orbit close to its unstable manifold. This observation makes sense, as it would be expected that points close to the stable manifold of an unstable orbit would come closer to that orbit over time. The relationship with the stable manifold is even more clearly seen in frame *h* where the thrust has modified the trajectory so that the backward integration appears to lie on the stable manifold of the 3:4 orbit. The next intersection then lies nearly on top of the 3:4 orbit, just as the stable manifold would behave. Overall it is also interesting to observe the changes in the invariant manifolds of the resonant orbits over the range of Jacobi constants in the frames in Fig. 12. The invariant manifolds move from having relatively few intersections with themselves in frame *a* to possessing the large number of intersections at many resonances seen in frame *h*. The optimization algorithm appears to be using low thrust both to move the intersection of the trajectory around the Poincaré section as well as to move to different energies where the invariant manifolds are located in positions that may be used by the trajectory.

Following the Invariant Manifolds at Nearly Constant *C*

In frames *i* through *n* of Fig. 12, the series of plots begins with the backward integrated point located near the previous location of the forward integrated point. This switch often occurs when the trajectory passes through the surface of section. The forward integrated point now lies nearly on the unstable manifold of the 3:4 orbit. This makes sense, as the backward integrated point actually lies just off the 3:4 orbit on its unstable manifold, and the next intersection is naturally further away from the 3:4 orbit on the unstable manifold. As time continues, the thrust is used to move the backward integrated point slightly toward the stable manifold of the 5:6 orbit. As this is done, the forward integrated point moves backward along the unstable manifold of the 3:4 orbit in the Poincaré section. It then continues to generally follow the unstable manifold of the 3:4 orbit which lies very near the unstable manifold of the 5:6 orbit. These frames correspond to the series of points shown earlier in Fig. 11. Remember that it is the optimization algorithm that has selected this path for the trajectory, and it is very interesting that nearly all the points in the sequence lie very near the unstable manifold. It indicates that the optimization algorithm has converged on the invariant manifolds as optimum pathways between resonances.

Resonance Transition

Frames *o* through *t* of Fig. 12 continue the sequence starting at the next major thrusting period. The first five frames at the beginning of this thrusting period reveal significant changes in the location of the forward integrated point as it appears to move from the 3:4 resonance in the previous sequence of plots to the 5:6 resonance along the unstable manifolds of the 3:4 and 5:6 orbits. Through this process, the backward integrated point moves slightly along the stable manifold of the 5:6 orbit as it begins to approach the 5:6 orbit. As before, it is not unexpected that the fact that the backward integrated point lies near the stable manifold of the 5:6 orbit would produce a forward integrated point that is then closer to the general vicinity of the 5:6 orbit. The fact that the forward integrated point lies near the unstable manifolds of both the resonant orbits is curious. Integrating the point on the stable manifold of the 5:6 orbit closest to the backward integrated point shows that the next intersection of the stable manifold is nearly on top of the 5:6 orbit. So the slight difference in initial conditions between the stable manifold of the 5:6 orbit and the backward integrated point results in a large difference in the location of the next intersection. Overall, this sequence of plots aids in revealing the method by which the optimization scheme has used low thrust to perform a resonance transition. In frame *t*, the backward integrated point continues to move along the stable manifold of the 5:6 orbit, and the forward integrated point moves past the 5:6 resonance. Beyond this time period, the trajectory begins the approach phase at Europa using a DRO. Further analysis at this point requires the selection of a new surface of section, because the current surface of section is on the opposite side of Jupiter from the DRO.

[§]Note that the same color convention used in Fig. 11 applies to all of the Poincaré sections. The labels are typically not shown so that the manifolds are not obscured.

Conclusions

This study has revealed the close link between an optimized low-thrust trajectory transitioning across resonances and the invariant manifolds of unstable resonant orbits. The link was discovered by observing that the intersections of the trajectory in the Poincaré sections closely followed the invariant manifolds of the resonant orbits, despite the fact that the optimization algorithm had no knowledge of the existence of the invariant manifolds. This relationship was found to persist across energy levels and over thrusting periods, which indicates the two primary ways in which the optimization algorithm manipulated the trajectory. In one case, the algorithm modified the energy of the trajectory through thrusting to a level where the invariant manifolds were more suitably placed to allow resonance transitions. At other times, the thrusting was primarily used to move the trajectory along the invariant manifolds toward the desired resonance. These results indicate that resonant orbits and their invariant manifolds may be fundamentally important for understanding the optimal pathways that may be used by low-thrust trajectories. Knowledge of this relationship has the potential to be very useful in developing initial guesses for these optimization algorithms, and ultimately it should aid in developing control laws for new optimization algorithms that could find pathways for low-thrust trajectories using invariant manifolds.

Acknowledgments

Many thanks to Try Lam and Greg Whiffen for supplying the low-thrust trajectory developed in Mystic. Thanks also to Greg Whiffen for adapting his Mystic code to the circular restricted three-body problem for the trajectory and for his consultations on Mystic. The authors would like to thank George Born and Bob Easton for their support and their many helpful discussions. This work was conducted in part at the Jet Propulsion Laboratory, California Institute of Technology, under contract with NASA. It was supported in part by the Prometheus Project as well as the Episode Project and the MTool Project of the NASA Advanced Information Systems Research Program. The parallel computation used in this investigation was provided by the Jet Propulsion Laboratory Supercomputer Project and the Jet Propulsion Laboratory Supercomputing and Visualization Facility.

References

[1] Whiffen, G. J., "Static/Dynamic Control for Optimizing a Useful Objective," U.S. Patent 6,496,741, 17 Dec. 2002.

[2] Whiffen, G. J., "An Investigation of a Jupiter Galilean Moon Orbiter Trajectory," American Astronautical Society Paper 03-544, Aug. 2003.

[3] Whiffen, G. J., "Mystic: Implementation of the Static Dynamic Optimal Control Algorithm for High Fidelity Low Thrust Trajectory Design,"

AIAA Paper 2006-6741, Aug. 2006.
[4] Lo, M. W., "The Interplanetary Superhighway and the Origins Program," *Aerospace Conference Proceedings (2002)*, Vol. 7, Inst. of Electrical and Electronics Engineers, New York, 2001, pp. 3543–3562.
[5] Lo, M. W., Anderson, R. L., Whiffen, G., and Romans, L., "The Role of Invariant Manifolds in Low Thrust Trajectory Design (Part I)," American Astronautical Society Paper 04-288, Feb. 2004.
[6] Anderson, R. L., and Lo, M. W., "The Role of Invariant Manifolds in Low Thrust Trajectory Design (Part II)," AIAA Paper 2004-5305, Aug. 2004.
[7] Lo, M. W., Anderson, R. L., Lam, T., and Whiffen, G., "The Role of Invariant Manifolds in Low Thrust Trajectory Design (Part III)," American Astronautical Society Paper 06-190, Jan. 2006.
[8] Anderson, R. L., "Low Thrust Trajectory Design for Resonant Flybys and Captures Using Invariant Manifolds," Ph.D. Thesis, University of Colorado at Boulder, CO, 2005, http://ccar.colorado.edu/~rla/papers/andersonphd.pdf.
[9] Lawden, D. F., *Optimal Trajectories for Space Navigation*, Butterworths, London, 1963.
[10] Betts, J. T., and Erb, S. O., "Optimal Low Thrust Trajectories to the Moon," *SIAM Journal on Applied Dynamical Systems*, Vol. 2, No. 2, 2003, pp. 144–170. doi:10.1137/S1111111102409080
[11] Betts, J. T., "Survey of Numerical Methods for Trajectory Optimization," *Journal of Guidance, Control, and Dynamics*, Vol. 21, No. 2, March–April 1998, pp. 193–207. doi:10.2514/2.4231
[12] Whiffen, G. J., and Lam, T., "The Jupiter Icy Moons Orbiter Reference Trajectory," American Astronautical Society Paper 06-186, Jan. 2006.
[13] Vavrina, M., and Howell, K. C., "Global Low-Thrust Trajectory Optimization Through Hybridization of a Genetic Algorithm and a Direct Method," AIAA Paper 2008-6614, Aug. 2008.
[14] Howell, K. C., and Ozimek, M. T., "Low-Thrust Transfers in the Earth-Moon System Including Applications to Libration Point Orbits," American Astronautical Society Paper 07-343, Aug. 2007.
[15] Dellnitz, M., Junge, O., Post, M., and Thiere, B., "On Target for Venus–Set Oriented Computation of Energy Efficient Low Thrust Trajectories," *Celestial Mechanics and Dynamical Astronomy*, Vol. 95, Nos. 1–4, 2006, pp. 357–370. doi:10.1007/s10569-006-9008-y
[16] Szebehely, V., *Theory of Orbits: The Restricted Problem of Three Bodies*, Academic Press, New York, 1967, pp. 7–41.
[17] Roy, A. E., *Orbital Motion*, 3rd ed., Adam Hilger, Philadelphia, 1988, pp. 111–163.
[18] Murray, C. D., and Dermott, S. F., *Solar System Dynamics*, Cambridge Univ. Press, Cambridge, England, U.K., 1999, pp. 421–428.
[19] Wiggins, S., *Introduction to Applied Nonlinear Dynamical Systems and Chaos*, Vol. 2, Texts in Applied Mathematics, 2nd ed., Springer–Verlag, New York, 2003, pp. 28–70.
[20] Parker, T., and Chua, L. O., *Practical Numerical Algorithms for Chaotic Systems*, Springer–Verlag, New York, 1989, pp. 130–166.
[21] Masdemont, J., and Mondelo, J. M., "Notes for the Numerical and Analytical Techniques Lectures" (draft version), Advanced Topics in Astrodynamics Summer Course, Barcelona, July 2004, http://www.ieec.fcr.es/astro04/notes/analnum.pdf.
[22] Lam, T., "Ganymede to Europa in Mystic's Circular Restricted Three Body Model," Interoffice Memo, Jet Propulsion Lab., Europa Orbiter Project Archive, Pasadena, CA, Oct. 2004.
[23] Lam, T., and Whiffen, G. J., "Exploration of Distant Retrograde Orbits Around Europa," American Astronautical Society Paper 05-110, Jan. 2005.
[24] Howell, K. C., and Breakwell, J. V., "Three-Dimensional, Periodic, 'Halo' Orbits," *Celestial Mechanics*, Vol. 32, No. 1, Jan. 1984, pp. 53–71.